5

Methods for Gully Characterization in Agricultural Croplands Using Ground-Based Light Detection and Ranging

Henrique Momm, Ronald Bingner, Robert Wells and Seth Dabney
USDA-ARS-National Sedimentation Laboratory
United States of America

1. Introduction

Soil erosion has long been recognized as the primary cause of soil degradation in agricultural fields (Wells et al., 2010). Overland flow in agricultural fields is the main process associated with soil erosion, which is often grouped into categories of: sheet erosion, rill erosion, and gully erosion (Smith, 1993). Traditionally, research has focussed on understanding and modelling sheet and rill erosion processes (Poesen et al., 1996). Recent research has begun to focus on addressing gully issues such as the understanding of the formation of gullies, their contribution to overall soil loss, development of tools to locate channel initiation, and appropriate measuring techniques (Poesen et al., 2003). The increased focus on gully research can be partially attributed to recent studies demonstrating that gully formation is very common on cropland, especially in conventional tillage systems (Gordon et al., 2008) and can be as significant as sheet and rill erosion in terms of sediment yield (Bingner et al., 2010). Without a good understanding of gully processes, technology cannot be developed that can provide information needed by watershed managers when evaluating and implementing effective conservation practice plans.

Gullies can be generally classified as ephemeral, classical, or edge-of-field. The Soil Society of America (2001) defines ephemeral gully as "small channels eroded by concentrated flow that can be easily filled by normal tillage, only to reform again in the same location by additional runoff events". As the headcut migrates upstream and the channel gets wider, faster than the interval between farming tilling operations, farming equipment is forced to operate around the gully and as result the gully becomes permanent (classical gully). Finally, as the name suggests, edge-of-field gullies are defined by channels where concentrated flow crosses earth bank (Poesen et al., 2003).

New methodologies are being researched to understand gully formation and estimate sediment yield (Souchere et al., 2003, Cerdan et al., 2002, and Woodward, 1999). Studies use Digital Elevation Models (DEMs) as the basis to formulate theories explaining the relationship between field topography and gully occurrence (Woodward, 1999, Parker et al., 2007, and Cerdan et al., 2002). These efforts greatly benefit from accurate and detailed topographic information which can aid in the understanding of where and when gullies form and how these features evolve over time (headcut migration).

Despite the availability of DEMs at regional and local scales (spatial resolution ranging from 1 to 30 meters), these datasets often do not offer the necessary spatial and/or temporal

resolution for gully investigations at individual plot scale. In order to capture the micro-topography impacting gully formation and development over time it is necessary to work with DEMs with spatial resolution ranging between 5mm to 15cm (Schmid et al., 2004). Additionally, ephemeral and classical gullies are affected by precipitation events, management and conservation practices, crop phenology, and crop canopy development. In ephemeral gully investigations, timing becomes significant as farming practices can remodel the field's topography by filling the gully channel. Classic gullies are also dynamic, responding to condition changes through headcut migration, deepening, and channel widening processes. Standard DEM datasets produced either by government agencies on a national scale or by private companies on a regional scale can only capture a snap shot in time of gully development.

Recent developments in laser scanner technology provide new opportunities for scientific investigation of gullies located in croplands. Although, laser scanners have been previously used in similar investigations such as large-scale classical gullies in different locations such as mountain-side sites (Perroy et al., 2010), forest sites (James et al., 2007), desert sites (Park, 2008), and landslides (Hsiao et al., 2003 and Roering et al., 2009), its application to ephemeral and classical gully investigation is in the early stages of development. Ground-based laser scanners provide the tools for detailed multi-temporal analysis of micro-topography of gullies. With this detailed information it is possible to obtain digital terrain models (catchment area, slope, planform curvature, thalweg, and cross sections), estimate soil roughness, perform volume calculations, and others. This is especially important in research setups where the same location needs to be surveyed multiple times over extensive periods of time as conditions change due to rain events, field management changes, and/or different conservation practices investigations. Ground-based laser systems are capable of providing high levels of topographic and morphologic details.

Ground-based light detection and ranging (LiDAR) systems differ from airborne systems. During data collection, the scanner (LiDAR sensor) is located on a tripod at ground level (Figure 1). Proximity to the ground surface causes laser pulses to be sent with larger range of vertical incidence angles than the airborne system. Ground sampling density is influenced by operator controlled factors such as investigation area selection (vertical and horizontal incidence angles), instrument resolution (average point density at mid-range), and degree of overlap between scans. The large volume of points combined with irregular point distribution of ground-based LiDAR data sets makes production of digital elevation models computationally challenging. Additionally, the presence of vegetation, standing residues, and shadows (regions with no data) represents an extra level of complexity that often cannot be addressed by standard off-the-shelf commercial geospatial software packages.

In this chapter, we describe new and enhanced techniques to pre-process and evaluate detailed topographic information acquired with ground-based LiDAR, which were specifically devised to quantitatively and morphologically characterize gullies located in agricultural fields. In the following section (Section 2) background information about ground-based LiDAR systems is provided. In section 3, multiple techniques to pre-process LiDAR data in the original point cloud format are depicted, such as cross-validation between scans (geo-referencing accuracy investigation), point sampling pattern investigation in terms of density (quadrant methods) and spatial distribution (distance to nearest neighbours), removal of unwanted points (thinning and outlier removal), and surface reconstruction (surface smoothing). Morphological analysis through cross-section

investigation follows in Section 4. An alternative method to overcome the high computational cost involved in the conversion of large point cloud into raster grid is addressed in Section 5. We provide a brief description of the implementation details as well as the computer programming language libraries utilized in Section 6. A study case of a gully located in a field of the Cheney Lake Reservoir Watershed (in South Central Kansas, USA) is included in Section 7 to illustrate some the techniques previously described. The chapter ends with discussion of the importance of this work and points to future research needs (Section 8). The material in this chapter can be used as a basis to develop guidelines on the use of ground-based LiDAR technology to characterize topographic conditions associated with the formation and evolution of agricultural gullies at field scale. This is especially important in research sites where the same geographical location needs to be surveyed multiple times over lengthy periods of time as conditions change due to precipitation and runoff events, field management, and implementation of conservation practices.

Fig. 1. Ground-based LiDAR utilized for gully formation and evolution studies in agricultural croplands.

2. Light detection and ranging technology

LiDAR technology, measures the laser pulse travel time from the transmitter to the target and back to the receiver allowing the distance to be calculated (Wehr and Lohr, 1999). In this process, a very accurate timing system is needed to guarantee an accurate resolution since laser pulses are sent at the rate of thousand times per second. Additionally, the transmitter and the receiver must be located at the same physical location, which is a single-ended system because the phase the incoming signal is compared to the phase of an internal clock at the same location (Measures R. M., 1984). This technology is often classified into air-borne and ground-based systems.

In airborne LiDAR systems, the aircraft position is recorded using accurate positional systems such as inertial navigation unit, GPS receivers located in the aircraft, and GPS base locations. With these combined equipment, it is possible to determine three-dimensional geo-referenced coordinates for each pulse and then correct for the aircraft positioning in terms of roll, pitch, and heading, thus improving the accuracy of the system.

Ground-based LiDAR systems, are simplified because the sender/receiver's location is known. They operate in a similar fashion to the reflectorless total stations. For each pulse, these systems can measure: (1) x, y, z coordinate values with respect to the position of the laser sensor; (2) the intensity of the returned signal as reflectance; and (3) RGB values from an integrated digital camera within the instrument.
These systems are capable of collecting information with a wide range of ground sampling densities as a result of operator controlled factors such as scan angle (area covered by individual scans), average point density, and degree of overlap between scans. Higher point density can be achieved by higher sensor resolution, smaller vertical field of view angles, and multiple scans of the same ground location. The instrument resolution is often controlled by an imaginary plane located at the middle range of the vertical field of view and is orthogonal to the sensor's normal sight. The vertical field of view angles also influence the point density as point sampling becomes sparser as vertical scan angles tends to the horizon. Multiple scans can be used to collect data over the same geographical location resulting in increased sampling density and overcomes problems such as shadowing and limited coverage due to vegetation.

3. Techniques to pre-process topographic information

Pre-processing is an important step introduced in a topographic data analysis scheme to minimize the influence of unwanted points and to maximize the influence of the desired ones, thus simplifying the computational work needed in the later stages of the analysis process in order to reach the investigation goals. Pre-processing is composed of operations such as filtering, enhancing, transformation, or combination of these processes. The pre-processing techniques described herein include: cross-validation to assess geo-referencing accuracy between multiple scans of the same geographical location, investigation of point sampling patterns through quadrant method, evaluating the internal distribution of points using the average distance to the nearest neighbour, unwanted point removal, and surface reconstruction through surface smoothing.

3.1 Cross-validation

During field surveys, such as the one conducted a field in the Cheney Lake watershed in Kansas, the same geographical location can be covered by different scans. This technique is often used to increase sampling density and to avoid problems such as shadowing and limited coverage due to vegetation. The overlap in LiDAR point sampling can also be used to evaluate survey final geo-referencing accuracy. Since each individual scan is collected using local coordinates, geo-referencing is the procedure to convert from local coordinate system into global coordinate system.
Given that the overlapping scans collected have sufficient point density, neighbouring points can be identified, and elevation differences between these points can be determined. Similar approach is used to evaluate the accuracy of airborne LiDAR sensors by comparing elevation values of nearby points collected by different flight paths in overlapping areas. For each combination of two scans, points were analysed to form a list of neighbouring points. For illustration, consider two scans s^i and s^j where: $i \neq j$. A pair of points P^i_{xyz} and P^j_{xyz} are recorded into the list when two conditions are met: a) the points are from different scans $i \neq j$ and b) the horizontal distance between the two laser points is smaller than the distance threshold $\left(d < d_{threshold}\right)$.

For example, in Figure 2, scans 4, and 12, 13, 14, and 15 overlap. Scans 12, 13, 14, and 15 were designed to increase point sampling at the main gully channel. Each of these scans is geo-referenced using a set of four pre-registered targets (the global coordinates of the targets are known prior to the geo-referencing procedure).

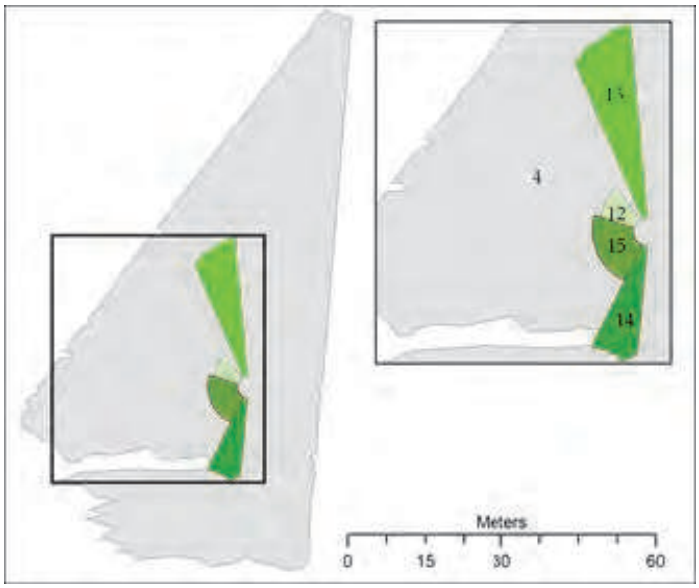

Fig. 2. Overlapping scans exemplifying the cross-validation procedure.

Using the cross-validation method for each pair of overlapping scans produces the tabular information presented in Figure 3. These values represent the upper quartile of the elevation difference between pairs of near points from different scans, multiplied by 1000. The values highlighted in Figure 3 exemplify geo-referencing problems between scans 4 and 12, 13, 14, and 15. Upon verification of the coordinates of the four targets used to geo-reference scans 12, 13, 14, and 15; the target with the largest RMS error was removed. A new cross-validation assessment between scan 4 and 12, 13, 14, and 15 was performed yielding new values of 17, 13, 16, and 17 respectively.

3.2 Quadrant method

A simplified and efficient way of exploring point pattern (spatial distribution and density) is to partition the location surveyed into sub-regions of equal area, or quadrants and then sum the number of laser points in each of the quadrants (Bailey and Gatrell, 1995). The division of the number of points by the area of the quadrant grid generates a measure of sampling intensity or laser points sampling density. The density map represents a two-dimensional frequency distribution (Bailey and Gatrell, 1995). This can be used to identify locations with high and low density, providing guidance to evaluate over and under-sampled areas. The density information can be correlated with topographic and land cover information for identification of areas with no laser point sampling due to shadowing and the influence of vegetation cover in the density information.

Scan	1	2	3	4	5	6	7	8	9	10	11	12	13	14	15	16	17	18	19	20	21	22
1	0																					
2	14	0																				
3	12	0	0																			
4	0	0	2	0																		
5	0	0	0	9	0																	
6	0	0	0	9	2	0																
7	0	0	0	9	5	0	0															
8	0	0	0	12	0	0	0	0														
9	0	0	0	12	0	0	4	0	0													
10	0	0	0	13	0	0	0	6	0	0												
11	0	0	0	16	0	0	0	6	0	3	0											
12	0	0	0	97	117	0	73	0	59	0	0	0										
13	0	0	0	69	0	0	0	60	0	40	0	0	0									
14	0	0	0	149	0	0	0	148	0	147	130	0	0	0								
15	0	0	0	88	0	0	0	92	0	84	0	0	3	30	0							
16	0	0	0	20	0	0	0	0	0	0	13	0	0	0	0	0						
17	0	0	0	21	0	0	0	18	0	17	17	0	0	161	0	3	0					
18	0	0	0	32	0	0	0	0	0	0	23	0	0	0	0	13	7	0				
19	0	0	0	0	0	0	0	0	0	0	0	0	0	0	0	0	0	0	0			
20	0	0	0	0	0	0	0	0	0	0	0	0	0	0	0	0	0	0	0	0		
21	0	0	0	26	0	0	0	0	0	0	28	0	0	0	0	18	0	0	0	0	0	
22	0	0	0	39	0	0	0	0	0	0	35	0	0	0	0	18	0	2	0	0	3	0

Fig. 3. Cross-validation values of the upper quartile obtained from the histogram of all the elevation difference between pairs of near points acquired from different scans (values in metres multiplied by 1000).

The quadrant method is influenced by the quadrant grid size. Larger quadrant grid sizes mask small density variations while small quadrant grid sizes create a larger range of density values with many quadrant grids containing no points. Using two different values of virtual quadrant grid, the gully represented by lighter colour in Figure 4A, is depicted by laser point sampling density associated with a virtual grid of 1.0 meter (Figure 4B) of 0.25 meter (Figure 4C). Both density maps reveal under-sampled locations.

3.3 Average distance to nearest neighbor

The use of the quadrant method provides the means to evaluate the spatial variation of the laser point sampling density. Density is often referred to as first order property of point pattern (Bailey and Gatrell, 1995). The use of the average distance to the nearest neighbours within each quadrant grid depicts an indication of the internal distribution of the laser points (Figure 5A). Based on this information binary maps can be generated of particular average distances (Figure 5B) to investigate sampling coverage. Although the average distance to the nearest neighbour provides an indication of how clustered or distributed laser points are in each quadrant grid, care should be used on analysis of large quadrant grids. In those analyses, two quadrants can produce the same average distance to nearest neighbour values, but one quadrant can contain a larger quantity of points uniformly distributed while the other quadrant contains fewer clustered points. To minimize this problem, a simple alternative is to combine the density map with the average distance to nearest neighbour map (Figure 5C).

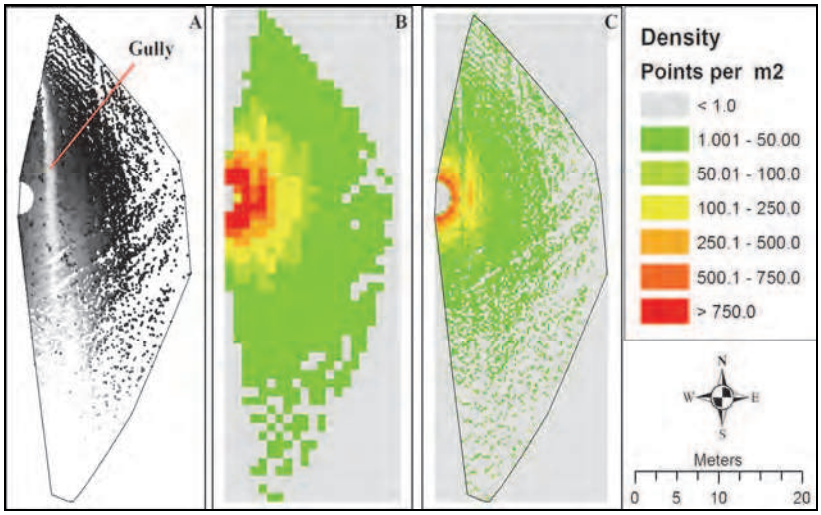

Fig. 4. Point pattern analysis using the quadrant method where the laser points (A) were sub-divided into quadrant grids of 1.0 and 0.25 meters (B and C respectively). The density map provides overall visualization of spatial variation of sampling density.

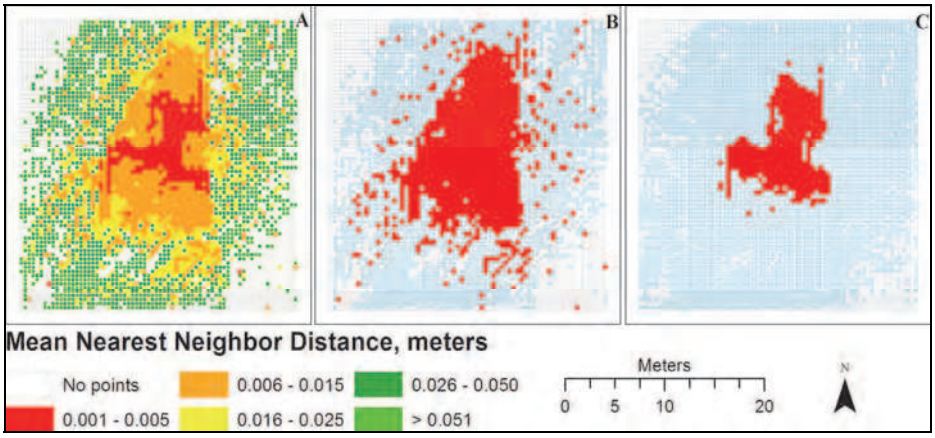

Fig. 5. (A) Average distance to the nearest neighbour of laser points within each quadrant grid. (B) Red symbology indicates the quadrant grids with average distance to nearest neighbour smaller than 1.5 cm. (C) Quadrant grids with average distance to nearest neighbour smaller than 1.5 cm containing greater than 500 laser points symbolized in red.

3.4 Thinning

Similarly to the quadrant method, thinning generates a two-dimensional virtual quadrant grid covering the entire extent of the point cloud, identifies the points within each quadrant, and keeps only the point with the lowest elevation in each quadrant. This technique, originally devised to filter trees out in order to obtain bare Earth data sets, is based on the

assumption that in surveys with enough sampling density, vegetated areas will have points that can penetrate the tree canopies and reach the ground. The same concept can be adopted when working with terrestrial laser scanners. Vegetation foliage and residue stubs can be partially removed by thinning procedure (Figure 6).

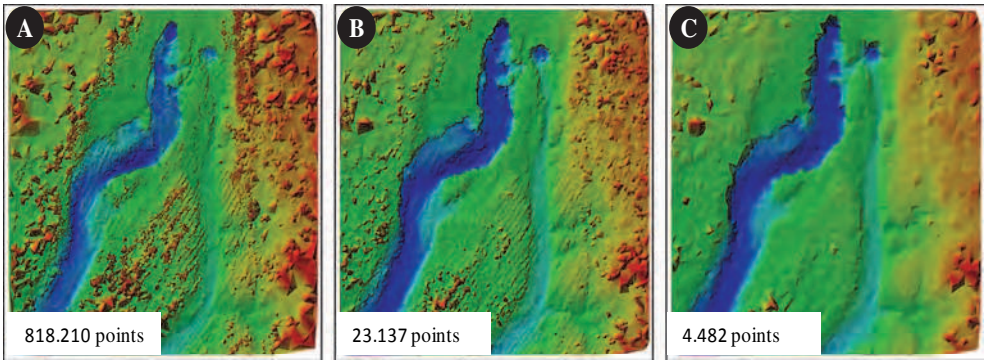

Fig. 6. Triangular Irregular Network (TIN) representation of point clouds before and after thinning procedure of a 18x18 meter section. The original surveyed section (A) is filtered through thinning using virtual grid cell sizes of 10 (B) and 25 cm (C), respectively.

3.5 Outlier removal

Gully investigations in cropland require artificial removal of outlier laser points to generate the true bare Earth representation. These points can constitute standing crop residue, vegetation canopy, or even individual incorrect registered scan lines. Two different approaches were considered here: square average distance (SAD) to the K-nearest neighbours (KNN) and distance to the fitted surface (DFS) to the KNN (Bäsken, 2010, Delage, 2010, Cazals and Pouget 2008). Unlike the previously described quadrant methods that compute two-dimensional distances, these two approaches classify a point as an outlier or not based on three-dimensional Euclidean distance.

In the SAD algorithm, for each point the K nearest neighbours are selected and the square average distance between these points is computed. If this value is larger than a user provided threshold the point is assigned to be removed. A subset of a gully channel with different outliers, standing crop residue (two sharp peaks) and small lines of elevated points were evaluated (Figure 7A). An initial attempt to remove these outliers used a square average distance threshold of 5 cm for the 50 nearest neighbours resulting in the removal of one point (Figure 7B). A second attempt using 10 nearest neighbours and a square average distance threshold of 1 cm removed an additional 14 laser points.

The DFS algorithm, identifies the K nearest neighbours for each laser point, fits a polynomial surface to these points, and computes the three-dimensional distance of the point being evaluated to the fitted surface. If the distance is greater than the user-specified threshold the point is then marked for removal. The polynomial order is also a parameter defined by the user. The same information shown in Figure 7A is filtered using a first order polynomial surface, planar surface, removing a total of 4312 points (Figure 7D). Visual comparison to the original dataset (Figure 7A) indicates the removal of most outlier points.

3.6 Smoothing

The presence of vegetation and/or standing crop residue can yield point clouds, and subsequently digital terrain representations, with large elevation variations (quantified by large standard deviations). In such noisy datasets, techniques can be devised for surface reconstruction (herein referred to as smoothing). The objective is to attenuate large local relief variations while maintaining the global relief of the terrain. Unlike the filtering procedures, no points are removed but rather three-dimensionally moved to a fitted surface to the KNNs of each point (Delage, 2010, Cazals and Pouget 2008). The output point cloud contains the same number of points than the original one, however, the coordinate values of each point is slightly modified. The parameters required are the k number of neighbours and the degree of the polynomial to generate the fitted surface. The lower the degree of the polynomial the smoother the reconstructed surface will be. The original surface (Figure 7A) can be reconstructed using a third order polynomial (Figure 7E) while a surface using a first order polynomial (plane) can also be constructed (Figure 7F). Visual inspection indicates a more realistic representation using the third order polynomial over than the first order.

3.7 Summary

Although the selection of the most appropriate algorithm along with their parameters varies according to the terrain (topography and land cover) and scale (flume, plot, or field), best results can be obtained by combining these procedures (filtering and smoothing). A list of the tools described in this section with the necessary inputs, the generated output, and the main purpose are listed in Table 1.

4. Morphological analysis

In scientific settings, different gullies are surveyed multiple times with the objective to capture a channel's dynamic changes. The objective is to quickly assess channel morphological changes such as headcut migration, widening, deepening, and deposition, as well as estimation of the volume of soil eroded/deposited. As the number of surveys increases and consequently the volume of data, an automated and standard procedure to extract key parameters is necessary.

4.1 Automated cross-section generation

Channel geometry can be quantified through a series of cross-sections. Although cross-section methods exist in commercial off-the-shelf Geographic Information Systems (GIS) software packages, the generation of a series of closely spaced cross-sections can become a time consuming process due to the necessary file format transformations (conversion of point cloud into either raster or TIN format) and the lack of automation (user has to define the individual location of each cross-section).

The procedure developed requires the user to define a centreline approximating the gully thalweg in the ESRI Shapefile file format and input parameters describing how the cross-sections will be generated (Figure 8A). The cross-section geometric parameters are: length of the cross-section, distance between cross-sections (*b* in Figure 8A), distance between points within the cross-section (*c* in Figure 8A), and search radius (*a* in Figure 8A). The final elevation for each point of the cross-section is defined by the Inverse Weighted Distance (IDW) algorithm (Equation 1).

$$z_{0.} = \frac{\sum_{i=1}^{s}\left(z_i \frac{1}{d_i^k}\right)}{\sum_{i=1}^{s}\left(\frac{1}{d_i^k}\right)} \tag{1}$$

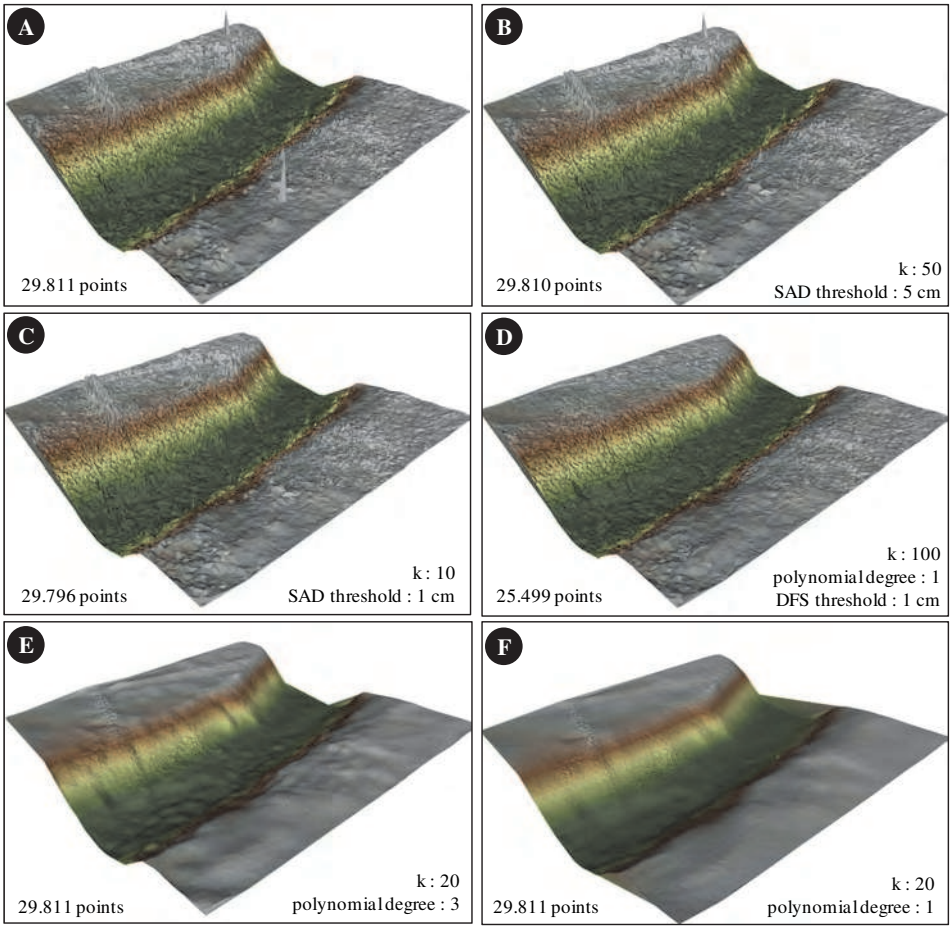

Fig. 7. Point cloud pre-processing algorithms: A – TIN representation of original point cloud; B – TIN representation of point cloud after outlier removal using a SAD of 5 cm and 50 KNN (k) points; C – TIN representation of point cloud after outlier removal using a SAD of 1 cm and 10 KNN points; D – TIN representation after outlier removal using distance to fitted surface (DFS) to KNN points (4312 points removed); E – TIN surfaces were reconstructed by three-dimensionally moving points to the surfaces fitted to the KNN points using a third order polynomial surface; and F – TIN surfaces were reconstructed by three-dimensionally moving points to the surfaces fitted to the KNN points using a first order polynomial surface.

The IDW algorithm is a local interpolation algorithm that assigns different weights to laser points based on their proximity to the unknown location (z_0). In Equation 1, the z_i is the elevation at the known point i, d_i is the distance between point i and the point being estimated (unkown location), and k is the power controling the degree of local influence (closer laser points are assigned higher weight) and is also an input parameter.

Module	Inputs	Outputs	Purpose
Cross-validation	• Two overlapping point clouds • Distance threshold	• List of 2D distances between selected pairs of points	Assessment of geo-referencing accuracy between overlapping scans
Quadrant method	• Point cloud • Virtual grid cell size	• Polygon feature class with laser point count for each polygon	Point sampling density investigation
Average distance to nearest neighbour	• Point cloud • Virtual grid cell size	• Polygon feature class with average distance to nearest neighbour of laser points within each polygon	Investigation of the spatial distribution of laser point within each virtual grid cell.
Thinning	• Point cloud • Virtual grid cell size	• Point cloud with reduced number of points	Filtering of vegetation and standing residue.
Square average distance to KNN	• Point cloud • Number of neighbours to consider • Degree of polynomial • Degree of Monge • Square average distance threshold	• Point cloud with selected laser points identified for removal	Filtering of unwanted laser points based on average distance to nearest neighbours.
Distance to fitted surface to KNN	• Point cloud • Number of neighbours to consider • Degree of polynomial • Degree of Monge • Distance threshold	• Point cloud with selected laser points identified for removal	Filtering of unwanted laser points based on 3D distance to fitted surface.
Smoothing	• Point cloud • Number of neighbours to consider • Degree of polynomial • Degree of Monge	• Modified point cloud where points were 3D moved.	Surface reconstruction.

Table 1. Summary of new and enhanced topographic information pre-processing tools developed for gully investigation in agricultural fields using ground-based LiDAR.

Based on using the same centerline and input parameters utilized in different surveys, gully channel geometrical changes between surveys can be quantified (Figure 9). The cross-sectional area difference between two cross-sections is computed by defining a reference elevation and computing the area of the closed polygon (red polygon in Figure 9). The change in cross-sectional area is determined by computing the difference between the individual cross-sectional areas . The thalweg is generated by simply connecting the point with the lowest elevation in each cross-section (Figure 10).

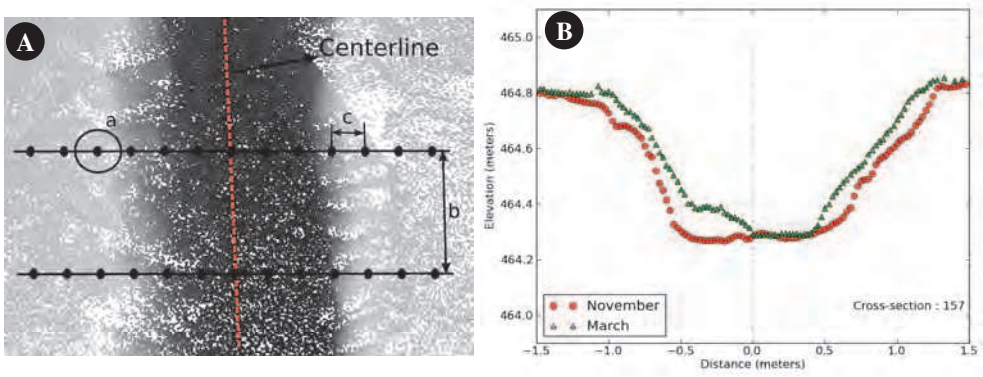

Fig. 8. (A) LiDAR point cloud with cross-sections generated. (B) Cross-section of a location at different periods of time.

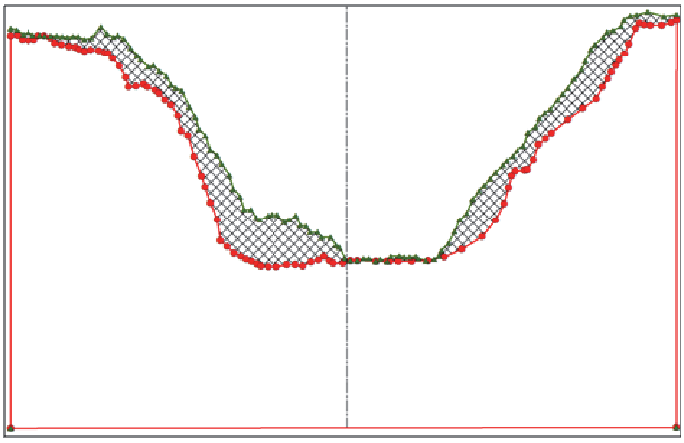

Fig. 9. Cross-sectional area generated with closed polygons by providing a base elevation.

4.2 Cross-section modeling

Quantification of gully channel geometrical properties is often performed by simplifying and fitting measured cross-sections through trapezoidal cross-section shapes. However, as the number of cross-sections grow as a result of gully channel extension, small cross-section interval, and high survey revisit time, identification of top-of-the-bank and channel toes

manually can become tedious and time consuming. Alternatively, a simplified optimization algorithm can be used to fit a trapezoidal cross-section to the LiDAR derived cross-section in a semi-automated fashion.

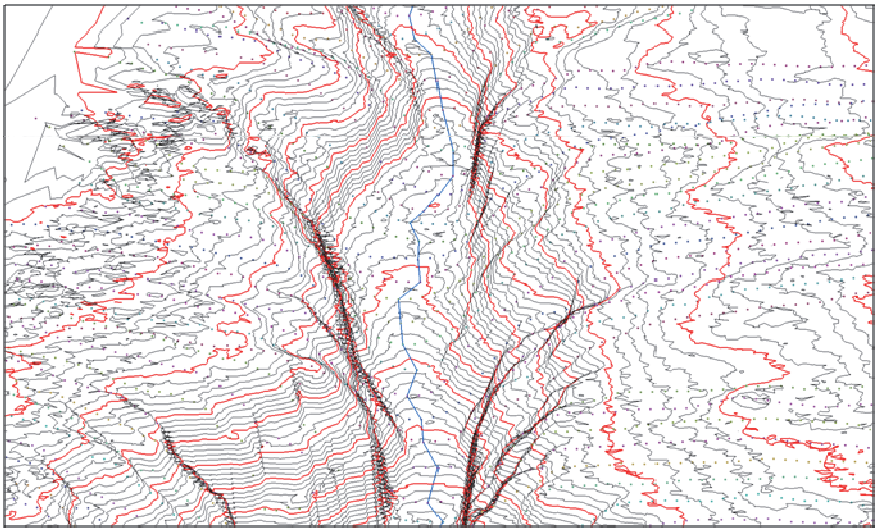

Fig. 10. Three-dimensional representation of the thalweg generated by connecting the cross-section point with the lowest elevation.

The algorithm iteratively fits two lines to each of the cross-section sides individually (left hand-side is shown in Figure 11). A series of scenarios are considered. Initially, the algorithm fits one line to the three points furthest from bank toe (blue points in Figure 11A) and another line to the remaining points (red points in Figure 11A). The root mean squared deviation (RMSD) of each of the fitted lines is computed and then the two combined (Equation 2). The process is repeated by increasing the number of points considered in the first line while reducing the points to the second line (Figure 11B), until only three points are left for the second line (Figure 11C). The optimum point is selected by identifying the minimum combined RMSD value trough minimization of Equation 2 (Figure 11D).

$$\text{Optimum Point} = \min imize\left\{\sqrt{\left(\sum_{i=1}^{i=j}\left[\left(Y_i - Y_i^a\right)^2\right] + \sum_{i-j+1}^{i=1}\left[\left(\left(Y_i - Y_i^b\right)^2\right)\right]\right)}\right\} \quad (2)$$

Where, Y_i^a is the elevation of the first fitted line *a* at point *i*, Y_i^o is the elevation of the second fitted line *b* at point *i*, *j* is the last point in the first set of points, and Y_i is the measured elevation at location *i*. A line is fitted to the gully bottom through least square error and the intercept of this line with the others generated with the optimization method (left and right banks) for a trapezoidal cross-section shape (Figure 12).

4.3 Summary

The main objective of the cross-section processes is to standardize and to expedite the cross-section generation and analysis. These procedures play an important role when conducting

multi-temporal investigations devised to quantitatively assess gully changes over time (formation and evolution). The main components described herein are listed in Table 2, along with their required input, output, and the main purpose.

Module	Inputs	Outputs	Purpose
Cross-section generation	• Point cloud • Centreline (feature class) • Cross-section length • Distance between cross-sections • Distance between points in the cross-section • Search radius • IDW power • Minimum number of points to consider	• Point feature class with X, Y, and Z coordinates of each cross-section point plus cross-section number	Gully channel geometry investigations.
Gully thalweg generation	• Point feature class generated using the cross-section module	• Polyline feature class	Gully thalweg investigations.
Cross-section area computation	• Point feature class generated using the cross-section module • Datum elevation	• Table listing area for individual cross-section	Multi-temporal investigation of cross-sectional area change.
Cross-section modelling	• Point feature class generated using the cross-section module	• Table listing line equations and intersection	Systematic extraction of geometric parameters from cross-section.

Table 2. Summary of tools implemented for gully morphological analysis in agricultural fields using ground-based LiDAR.

5. Interpolation using local binning algorithms

Point clouds generated using Ground-based LiDAR systems at field-scale and even at flume-scale can yield large datasets (millions of points) with varying sampling densities and uneven point distributions posing a challenge to interpolation techniques based on global estimates such as a regularized spline with tension and ordinary Kriging algorithms. The algorithm proposed by Kim (2006) was adopted and expanded to generate grids of intensity, red, green, and blue values in addition to elevation values. This algorithm produces a tree data-structure (Quadtree) point cloud designed to recursively partition the two-dimensional space (X and Y coordinates) to expedite queries of laser points in the desired neighbourhood (Bäsken, 2010).

6. Implementation

The described algorithms were implemented in a combination of C++ and Python computer programming languages as a result of the need to have customizable tools that were not previously available in GIS software packages.

The point clouds were stored and manipulated using the American Society of Photogrammetry and Remote Sensing (ASPRS) LASer file format (LAS) through the libLAS library (http://liblas.org/). To overcome the large point cloud size (millions of laser points) the Computational Geometry Algorithms Library (CGAL) was selected to perform efficient nearest neighbour queries (Delage, 2010), compute distances, outlier removal (Allez et al., 2010), normal estimation, and fitting of three-dimensional polynomial surfaces (Cazals and Pouget, 2008). The cross-section modelling algorithm was developed using the Scientific Tools for Python (SciPy) due to the plotting capabilities offered. Additionally, the ESRI Shapefile file format was used when generating/manipulating cross-sections and thalweg files.

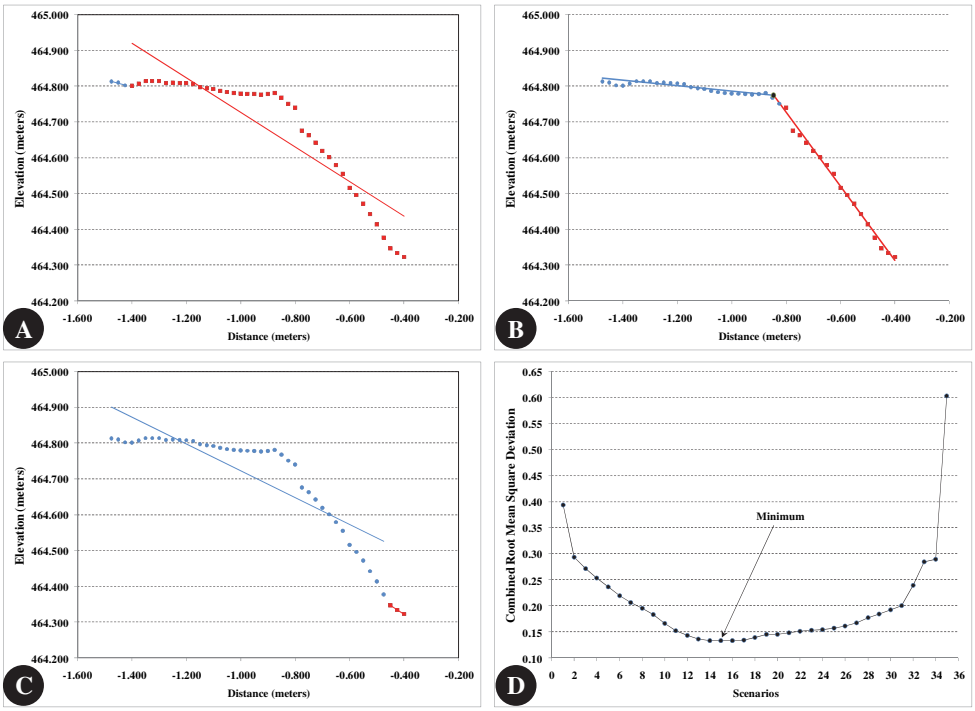

Fig. 11. Optimization procedures to fit a theoretical trapezoidal cross-section to the measured cross-section obtained with ground-based LiDAR points from Kansas field surveys. In the first scenario two lines are fitted, one to the first three points and the second to the remaining points (A). The procedure continues until the second line has only three points (C). The optimal fit is obtained by the minimum RMSD value (B) after all the scenarios are evaluated (D).

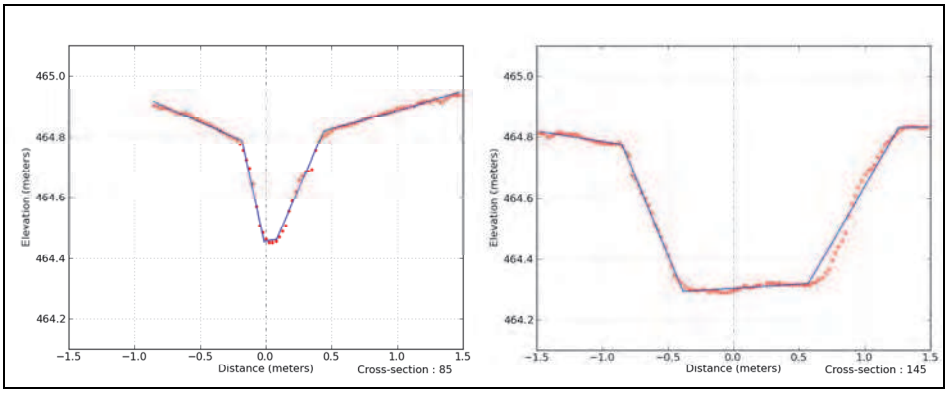

Fig. 12. Trapezoidal cross-sections fitted to measured data.

7. Study case

A gully located in South Central Kansas was selected for analysis. The gully is within the Cheney Lake Reservoir watershed and is approximately 96 metres long, 1.3 metres wide at the widest location, from 10 to 50 centimetres deep, and oriented North-South. The channel is free of vegetation and crop residues, while the surrounding field is covered by crop residues resulting from no-till management used in winter wheat followed by sorghum (milo) in the 2010 crop rotation. Historical cultivation practice records indicate that initially this gully did not disrupt farming operations; however, as no-tillage practices were adopted in 2005, the channel grew wider and deeper to the point that the farming equipment could not be used to travel across the gully and the ensuing cropping activity was performed around the main channel (Frees et al, 2010). The site was visited and surveyed in March and November of 2010. Measured precipitation records indicate two significant precipitation events occurred in June and July, 2010 (Figure 13).

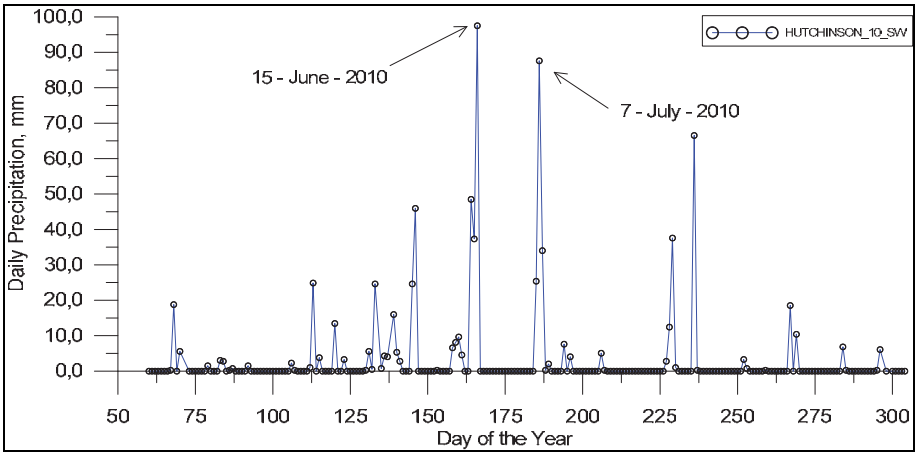

Fig. 13. Daily precipitation between March-2009 and November-2010 from a weather station located 4,5 Km from the field investigated.

The equipment used was a TOPCON GLS-1000 series that has a 4 mm single point accuracy distance (Table 3). The surveys are composed of 11 and 7 scans resulting in a total of 945,668 and 3,673,167 laser points for March and November, 2010, respectively. The surveys presented different laser point sampling densities (Figure 14). The survey conducted in March yielded higher variation in the sampling rate (density) in the gully channel with two clusters of high density. Conversely, the survey conducted in November generated a more uniform sampling rate specifically on the gully channel.

Parameter	Value	Unit	Condition
Single point accuracy distance	4.0	(σ) mm	1 to 150 meters
Single point accuracy vertical angle	6.0	seconds	1 to 150 meters
Single point accuracy horizontal angle	6.0	seconds	1 to 150 meters
Maximum scan rate	3000	Hz	
Scan density spot size	6.0	mm	1 to 40 meters
Scan maximum sample density	1.0	mm	up to 100 meters
Laser wavelength	1535	Nm	
Laser pulse duration	3.6	nano second	
Laser maximum pulse frequency	3400	Hz	

Table 3. General specifications of the TOPOCON GLS-1000 laser scanner

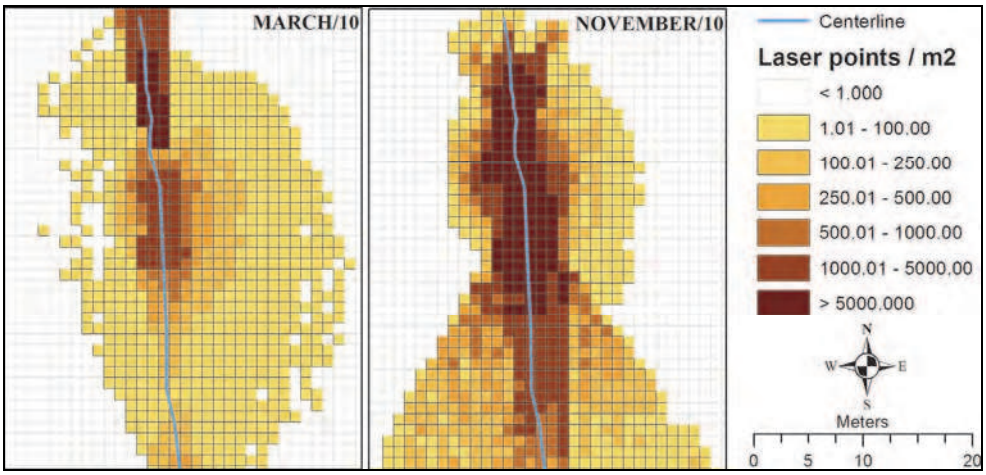

Fig. 14. Comparison of laser point sampling density between March and November, 2010 surveys.

Both surveys were subset to the same extent (gully only) to remove unwanted laser points regarding agricultural furrows and standing crop residues. Additional outliers were removed using the square average distance to KNN algorithm with threshold of 5 cm and *k* of 50 followed by a thinning algorithm using a virtual grid of 1.5 cm.

Using the local binning algorithm with a raster grid size of 2.5 cm, search radius of 5.0 cm and IDW power 2, two raster grids were generated (Figure 15). Areas were identified with elevation changes signifying different physical processes based on computing the difference

between the two grids. The active headcut migration path is represented by the darker blue colour indicating the occurrence of incision processes between cross-section 50 and 90 (Figure 15). Further downstream, between cross-sections 99 and 145 (Figure 15), the predominant physical process is widening of the gully channel as result of encountering a less erodible layer.

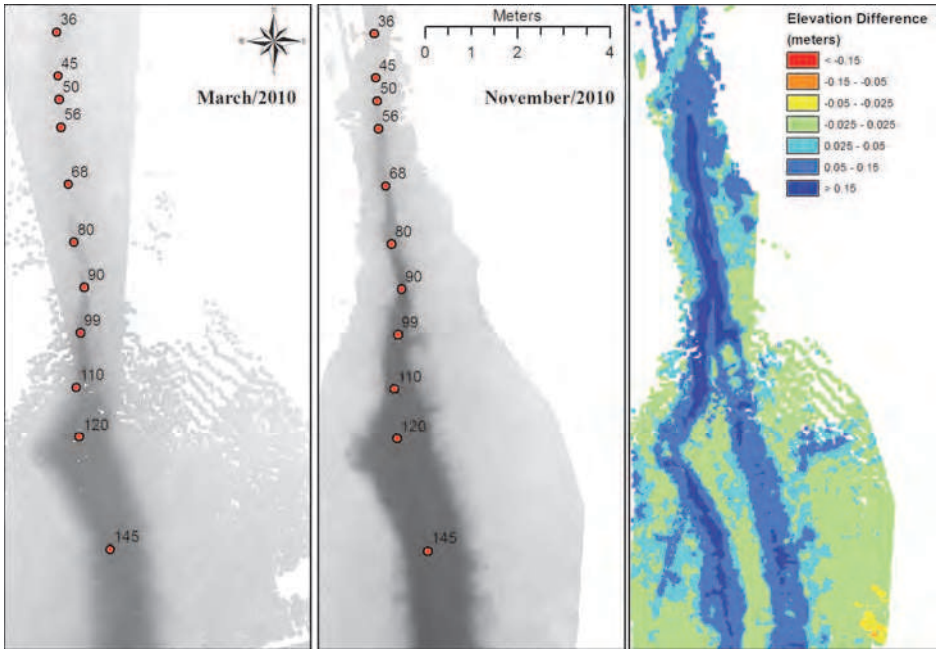

Fig. 15. Raster grid generated using local binning interpolation algorithm. Differencing of these grids illustrate elevation changes that occurred during the time period investigated. The red dots mark selected cross-sections.

Using the same user-provided centreline for both surveys a set of cross-sections were automatically generated and compared. Cross-sections at different locations of the gully were computed (Figure 16) based on various parameters (Table 4). A total of 448 cross-sections were generated for each survey varying in the extent and number of points as result of the non-uniform distribution of the laser points.

Parameter	**Value**
Cross-section size	3.0 meters
Distance between points in the cross-section	2.5 centimeters
Distance between cross-sections	10.0 centimeters
Power used in IDW	2.0
Search radius	5.0 centimeters

Table 4. Parameters considered in the generation of cross-sections for multi-temporal morphological analysis of gully evolution in croplands.

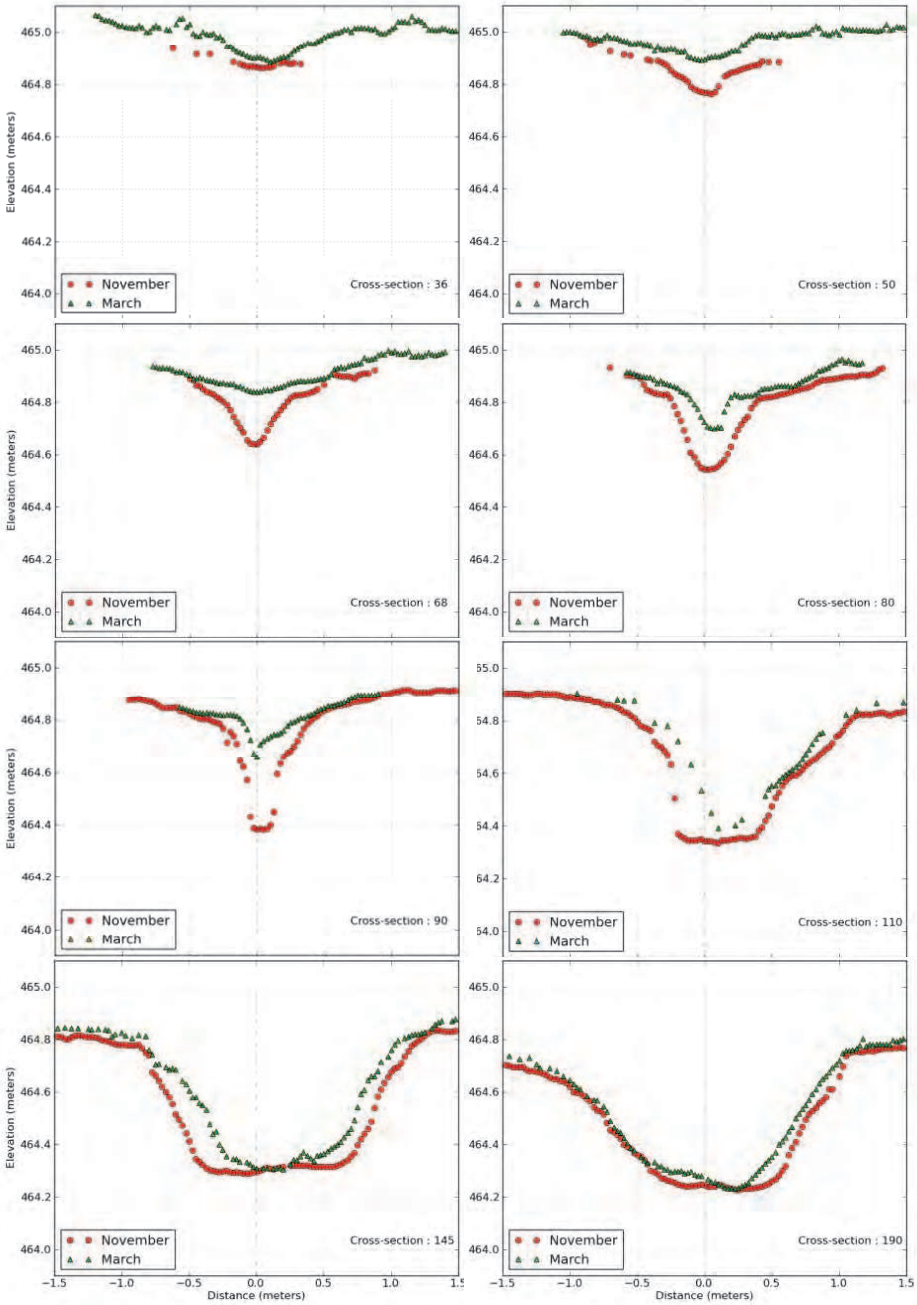

Fig. 16. Selected cross-sections measured in March and November of 2010.

The profiles, one for each of the surveys, were generated by deriving elevation information from the intersection of the user-defined centreline and each measured cross-section (Figure 17). Comparison between the two profiles indicates the rate of headcut migration (between distances 5 and 10) as well as the amount of incision in that section (Figure 15). Beyond 10 meters, the November profile (blue line in Figure 17) points to a situation of stable slope or a less erodible layer. The deposited material in March was likely removed as result of the large storm events.

Differences in cross-sectional area are plotted in Figure 18. Visual comparisons between the cross-section difference plot and the series of cross-sections identify erosional patterns. Between cross-section 70 and 90 the difference in cross-section area is attributed mainly by headcut migration and incision processes. From station 90 to 100 a combination of widening of the channel and incision are responsible for the differences in cross-section area. Beyond station 110 the change in cross-sectional area is mainly due to widening of the channel, 110-130 side walls only, 130-175 side walls and bed, and 175-250 widening of the channel bed.

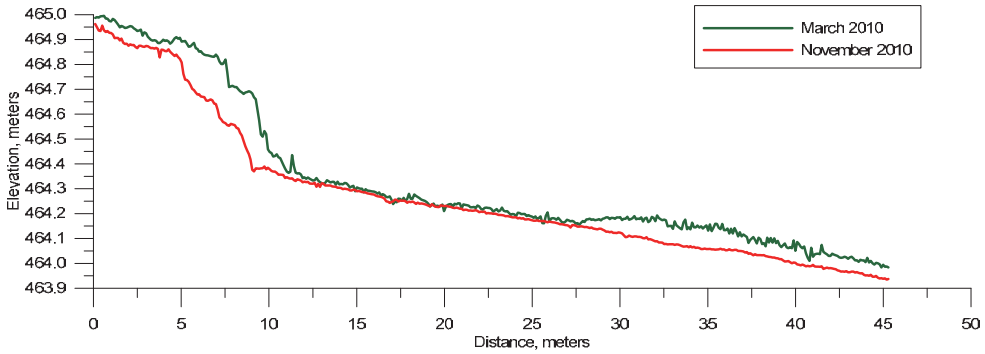

Fig. 17. User-defined centreline with Z elevation values obtained from the point of intersection with generated cross-sections for March (green) and November (red) of 2010.

8. Summary and closing remarks

The successful monitoring of gully evolution (ephemeral and classical) at individual gully scales in agricultural fields depends on accurate and detailed topographic information. The utilization of new technologies, such as ground-based LiDAR, provides new venues for scientific investigation of physical processes responsible for gully formation and evolution. Ground-based LiDAR can generate point clouds containing millions of points with point intervals varying from 1 mm to 200 mm depending on operator-defined parameters. These systems generate non-uniform spatial distributions of laser points (varying sampling density) because of the sensor's proximity to the target (equipment setup on tripods). The non-uniform distribution of points is influenced by relief, standing obstructions such as vegetation and crop residue, and vertical incidence angle. The format and massive amount of measured data represents a challenge for existing watershed modelling software applications that lack the necessary tools to pre-process the data and require the point clouds to be downgraded or interpolated in order to be used (Luccio, 2011). Watershed management planning will need these tools to implement economical and environmentally effective conservation practices.

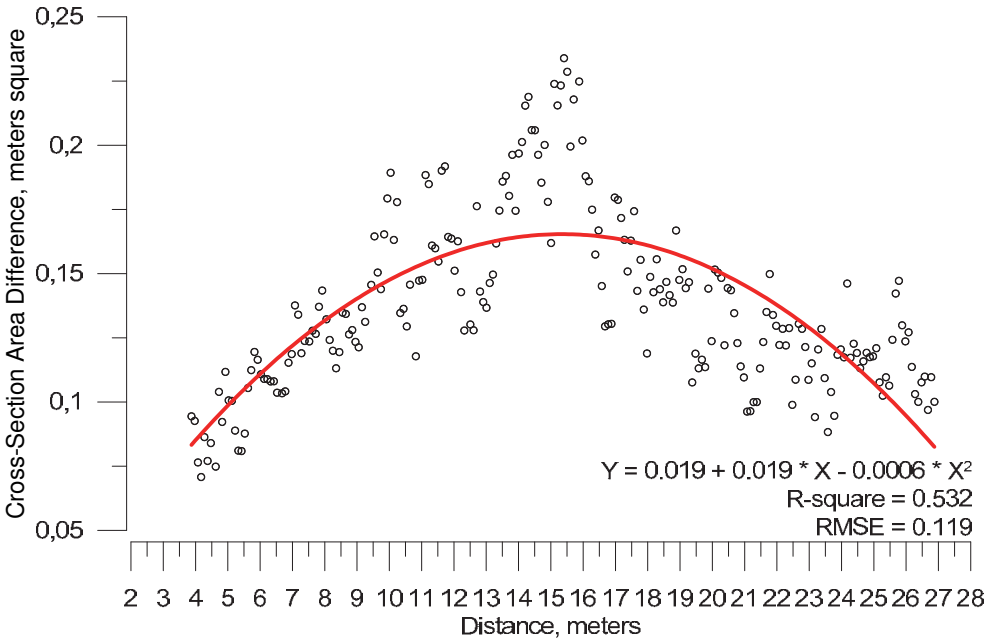

Fig. 18. Percentage change in cross-sectional area in square meters between March and November of 2010. Red curve represents the fitted second order polynomial function.

This chapter described a set of tools, devised primarily for gully investigation, to pre-process and extract morphological information from gully channels at different scales. These tools work with the point clouds in industry standard file format (LAS files) to minimize the need of file format conversions as well as to facilitate sharing between different systems. The tools also utilize advanced data structures and fitting algorithms to efficiently perform queries, compute distances between nearby laser points, and fit surfaces to KNNs, facilitating the removal of outlier points and the smoothing of the overall surface. Additionally, the extraction of morphological information in a semi-automated fashion was implemented through the analysis of cross-sections derived straight from the point clouds. This is an important feature providing a standard procedure to analyse multi-temporal data sets.

Future work includes the extension of the described system to include enhanced features such as classification of laser points based on elevation and intensity values, including combinations of each. In addition, correction of intensity values based on range and incidence angle, edge detection, and extraction of gully-specific geometric parameters are needed.

9. Acknowledgments

Acknowledgements are due to Lisa French and Howard Miller, at Cheney Lake Watershed, Inc., for contacting and coordinating with local land owners and for providing vital logistic

support. Thanks are also due to Don Seale and Antonia Smith for their indispensible assistance during data collection. Finally, the authors would like to acknowledge the technical suggestions and discussions offered by Dr. Langendoen.

10. References

Bailey T. C. & Gatrell, A. C. (1995). *Interactive Spatial Data Analysis*, Prentice Hall, England.

Bäsken, Matthias. (2010). 2D Range and Neighbor Search. In CGAL User and Reference Manual. CGAL Editorial Board, 3.7 edition. Accessed on: February 2011. Available from: <http://www.cgal.org/Manual/latest/doc_html/cgal_manual/packages.html#Pkg:PointSet2>

Bingner, R. L., Wells, R. R., Momm, H. G., Theurer, F. D., & Frees, L. D. (2010). Development and Application of Gully Erosion Components within the USDA AnnAGNPS Watershed Model for Precision Conservation, *Proceedings of 10th International Conference on Precision Agriculture*, July 18-21, Denver, Colorado, USA.

Cerdan, O., Souchère, V., Lecomte, V., Couturier, A. & Le Bissonnais, Y. (2002). Incorporating soil surface crusting processes in an expert-based runoff model: Sealing and Transfer by Runoff and Erosion related to Agricultural Management *Catena*, Elsevier, Vol. 46, pp. 189-205.

Delage, C. (2010). Spatial Sorting. In CGAL User and Reference Manual. CGAL Editorial Board, 3.7 edition, 2010. Date of access: February 2011, Available from: <http://www.cgal.org/Manual/latest/doc_html/cgal_manual/packages.html#Pkg:SpatialSorting>

Cazals, F. & Pouget, M. (2008). Algorithm 889: Jet_fitting_3:---A Generic C++ Package for Estimating the Differential Properties on Sampled Surfaces via Polynomial Fitting. *ACM Transactions on Mathematical Software*, Vol. 35 No. 3, pp. 1-20.

Frees, L. D., Theurer, F. D., Bingner, R. L., & French, L. (2010). Cheney Lake CEAP Project: Validation/Calibration, Nutrients. *Proceedings of 9th Federal Interagency Sedimentation Conference*, Las Vegas, NV, June 27 – July 1.

Gordon, L. M., Bennett, S. J., Alonso, C. V., & Bingner, R. L. (2008) Modelling long-term soil losses on agricultural fields due to ephemeral gully erosion. *Journal of Soil and Water Conservation* Vol. 63, No. 4, pp. 173-181.

Hsiao, K.; Liu, J.; Yu, M. & Tseng, Y. (2004). Change detection of landslide terrains using ground-based lidar data. *Proceedings of XXth ISPRS Congress,* Istanbul, Turkey, Commission VII, WG VII/5.

James, L. A.; Watson, D. G., & Hansen, W. F. (2007). Using LiDAR data to map gullies and headwater streams under forest canopy: South Carolina, USA. *Catena*, Elsevier Science, Vol. 71, pp. 132-144.

Kim, H., Arrowsmith, J. R., Crosby, C. J., Jaeger-Frank, E., Nandigam, V., Memon, A., Conner, J., Badden, S.B., Baru, C. (2006). An Efficient Implementation of a Local Binning Algorithm for Digital Elevation Model Generation of LiDAR/ALSM Dataset, Eos Trans. AGU, 87(52), Fall Meeting, San Francisco, CA, USA.

Luccio, M. (2011). LiDAR Update – Terrestrial Explodes, Software Still Lags, Imaging Notes, Winter, Vol. 26, No. 1, pp. 24-31.

Measures, R. M. (1984). *Laser Remote Sensing Fundamentals and Applications*. John Wiley & Sons, Inc.

Park, A. (2008) Evaluation of Terrestrial LIDAR for Monitoring Geomorphic Change at Archaeological Sites in Grand Canyon National, Technical Report of the United States Geological Survey. USGS, no. 1384.

Parker, C., Thorne, C., Bingner, R., Wells, R., & Wilcox, D. (2007). Automated Mapping of Potential for Ephemeral Gully Formation in Agricultural Watersheds Laboratory Publication, National Sedimentation Laboratory, No. 56.

Perroy, R., Bookhagen, B., Asner, G., & Chadwick, O. (2010). Comparison of gully erosion estimates using airborne and ground-based LiDAR on Santa Cruz Island, California *Geomorphology*, Vol. 118, pp. 288-300.

Alliez, P., Laurent, S., & Salman, N. (2010). Point Set Processing. In CGAL User and Reference Manual. CGAL Editorial Board, 3.7 edition. Accessed on November: 2010. Available from: <http://www.cgal.org/Manual/latest/doc_html/cgal_manual/packages.html#Pkg:PointSetProcessing>

Poesen, J. W., Nachtergaele, J., Verstraeten, G., & Valentin, C. (2003). Gully erosion and environmental change: importance and research needs. *Catena* Vol. 50, pp. 91-133.

Poesen, J. W., Vandaele, K., & Wesemael, V. (1996) Contribution of gully erosion to sediment production on cultivated lands and rangelands. *Erosion and Sediment Yield: Global and Regional Perspectives*, IAHS Publ. Vol. 236, pp. 251-266.

Roering, J. J., Stimely, L. L., Mackey, B. H., & Schmidt, D. A. (2009). Using DInSAR, airborne LiDAR, and archival air photos to quantify landsliding and sediment transport. *Geophysical Research Letters*, Amer Geophysical Union, Vol. 36, No. 19, pp. L19402.

Schmid, T., Schack-Kirchner, H., & Hildebrand, E. (2004). A case study of terrestrial laser-scanning in erosion research: calculation of roughness indices and volume balance at a logged forest site. *International Archives of Photogrammetry, Remote Sensing and Spatial Information Sciences*, Vol. 36, No. 8, pp. 114-118.

Smith, L. (1993) Investigation of ephemeral gullies in loessial soils in Mississippi. (GL-93–11), U.S. Army Corps of Engineers, Storming Media, Vicksburg, MS.

Soil Science Society of America. (2001). Glossary of Soil Science Terms. Soil Science of Americal, Madison, WI. Date of access: November 2010, Available from: <http::/www.soils.org/sssagloss/>.

Souchere, V., Cerdan, O., Ludwig, B., Le Bissonnais, Y., Couturier, A., & Papy, F. (2003). Modelling ephemeral gully erosion in small cultivated catchments. *Catena*, Elsevier, Vol. 50, pp. 489-505.

Wehr, A. & Lohr, U. (1999). Airborne laser scanning – An introduction and overview, ISPRS *Journal of Photogrammetry and Remote Sensing*, Vol. 54 No. 2-3, pp. 68-82.

Wells, R., Bennett, S., & Alonso, C. (2010). Effect of Upstream Sediment Inflow on the Morphodynamics of Headcuts. *2nd Joint Federal Interagency Conference*, Las Vegas, Nevada, USA, June 27 – July 1.

Woodward, D. (1999). Method to predict cropland ephemeral gully erosion. *Catena*, Elsevier, Vol. 37, pp. 393-399.

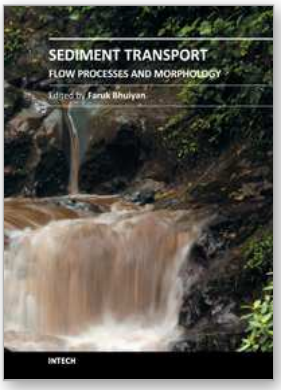

Sediment Transport - Flow and Morphological Processes
Edited by Prof. Faruk Bhuiyan

ISBN 978-953-307-374-3
Hard cover, 250 pages
Publisher InTech
Published online 26, October, 2011
Published in print edition October, 2011

The purpose of this book is to put together recent developments on sediment transport and morphological processes. There are twelve chapters in this book contributed by different authors who are currently involved in relevant research. First three chapters provide information on basic and advanced flow mechanisms including turbulence and movement of particles in water. Examples of computational procedures for sediment transport and morphological changes are given in the next five chapters. These include empirical predictions and numerical computations. Chapters nine and ten present some insights on environmental concerns with sediment transport. Last two contributions deal with two large-scale case studies related to changes in the transport and provenance of glacial marine sediments, and processes involving land slides.

InTech Europe
University Campus STeP Ri
Slavka Krautzeka 83/A
51000 Rijeka, Croatia
Phone: +385 (51) 770 447
Fax: +385 (51) 686 166
www.intechopen.com

InTech China
Unit 405, Office Block, Hotel Equatorial Shanghai
No.65, Yan An Road (West), Shanghai, 200040, China
中国上海市延安西路65号上海国际贵都大饭店办公楼405单元
Phone: +86-21-62489820
Fax: +86-21-62489821